LEF-1 drives aberrant β-catenin nuclear localization in myeloid leukemia cells

Rhys G. Morgan,[1,2] Jenna Ridsdale,[3] Megan Payne,[1] Kate J. Heesom,[4] Marieangela C. Wilson,[4] Andrew Davidson,[1] Alexander Greenhough,[1] Sara Davies,[3] Ann C. Williams,[1] Allison Blair,[1] Marian L. Waterman,[5] Alex Tonks[3] and Richard L. Darley[3]

[1]School of Life Sciences, University of Sussex, Brighton, UK; [2]School of Cellular and Molecular Medicine, University of Bristol, UK; [3]Department of Haematology, Division of Cancer and Genetics, School of Medicine, Cardiff University, UK; [4]University of Bristol Proteomics Facility, UK and [5]Department of Microbiology and Molecular Genetics, University of California, Irvine, CA, USA

©2019 Ferrata Storti Foundation. This is an open-access paper. doi:10.3324/haematol.2018.202846

Received: July 26, 2018.

Accepted: January 3, 2019.

Pre-published: January 10, 2019.

Correspondence: *RICHARD DARLEY* - darley@cardiff.ac.uk

RHYS MORGAN - rhys.morgan@sussex.ac.uk

Supplementary Table S1. Clinical characteristics of AML/MDS patient diagnostic/relapse samples used in this study.

Patient no.	Age (at diagnosis)	Sex	WBC count ($x10^9$/L)	Sample type	Secondary disease (Y/N)	Genetic information	Other clinical information
1	76	F	389	LP	N	Normal karyotype, $NPM1^+$, $FLT3^+$	n/a
2	4	M	n/a	BM	n/a	n/a	n/a
3	10	F	n/a	BM	n/a	n/a	Deceased
4	n/a	n/a	>200	PB	Y	n/a	Post-allogeneic transplant. M0/1 (previously diagnosed with M3 10 years previous)
5	6	M	n/a	BM	Y	n/a	Relapse
6	17	M	n/a	BM	Y	n/a	Post-BMT for AML following 2 relapses. Deceased
7	6	M	70.7	n/a	Y	n/a	Secondary to Ewings Sarcoma. Myelomonocytic morphology. Deceased.
8	14	F	7.6	BM	N	MLL rearrangement. Karyotype: 46,XX,ins(10;11)(q11.2;q23.1q23.3).ish ins(10;11)?inv(11)(q23.3)(5'MLL+)(q23.1)(3'MLL+)	BMT for high-risk AML
9	10	M	5.7	BM	N	Monosomy 7 secondary to GATA2 deficiency	BMT for MDS (Barth Syndrome)
10	43	M	16.1	BM	N	Normal karyotype	n/a
11	8	M	4.2	BM	N	t(8;21)(q22;q22) RUNX-RUNX1T1	Phenotype fits WHO criteria of MPAL. MRD negative post treatment course 1 and 2
12	4	M	3.2	BM	N	t(10;11)(p11.2;q23) KMT2A-MLLT10	High risk cytogenetics. BMT.
13	14	F	14.7	PB	N	t(8;21)(q22;q22) RUNX-RUNX1T1	MRD negative post treatment course 1 and 2
14	5	M	1.6	BM	N	n/a	M5. Deceased.
15	2	M	15.0	BM	N	t(8;21)(q22;q22) RUNX-RUNX1T1	n/a
16	8	F	n/a	BM	N	n/a	M4/5. Deceased.
17	7	F	34.4	BM	Y	MLL rearrangement t(9;11)	M5a morphology. BMT following relapse. Deceased
18	n/a	n/a	n/a	LP	n/a	n/a	n/a
19	6	F	20.6	BM	N	Normal karyotype	n/a
20	64	F	13.3	BM	N	Normal karyotype	AML with underlying MDS like changes
21	13	F	91.9	BM	Y	High Risk	Relapsed AML secondary to Rhabdoid tumour. Deceased

22	15	F	6.5	BM	N	MLL (KMT2A) rearrangement, t(10;11)(p11-p14,q23), MLL-MLLT10	MRD detected post treatment course 1
23	4	F	2.6	BM	N	Normal karyotype, $NPM1^{+}$	MRD neg
24	7	M	3.5	BM	N	t(8;21)(q22;q22) RUNX-RUNX1T1	
25	17	M	n/a	BM	N	t(15;17)(q24;q12)	
26	2	M	2.4	BM	N	t(9;11)(p22;q23), t(11;21)(q23;q8)	
27	14	F	2.1	BM	N	-7	BMT
28	11	M	n/a	BM	N	n/a	BMT for MDS. Deceased
29	7	F	n/a	BM	N	MPAL, 46XX, del5q, abnormal 21	
30	4mo	M	5.1	BM	N	t(9;11)	BMT
31	10	F	1.4	BM	N	n/a	
32	9	M	13.0	BM	N	Pericentric inversion of chromosome 16	90% blasts in BM, 73% blasts in PB
33	6	M	n/a	BM	N	n/a	

BM = Bone marrow
PB = Peripheral blood
LP = Leukapheresis
MRD = Minimal residual disease
BMT = Bone marrow transplant
AML= Acute myeloid leukemia
MDS= Myelodysplastic syndrome
MPAL= Mixed phenotype acute leukemia
MLL = *Mixed-lineage leukemia*
NPM1 = *Nucleophosmin*
FLT3 = *Fms-like tyrosine kinase 3*
RUNX1 = *Runt-related transcription factor 1*
GATA2 = *GATA Binding Protein 2*
WHO = World Health Organisation
n/a = not available

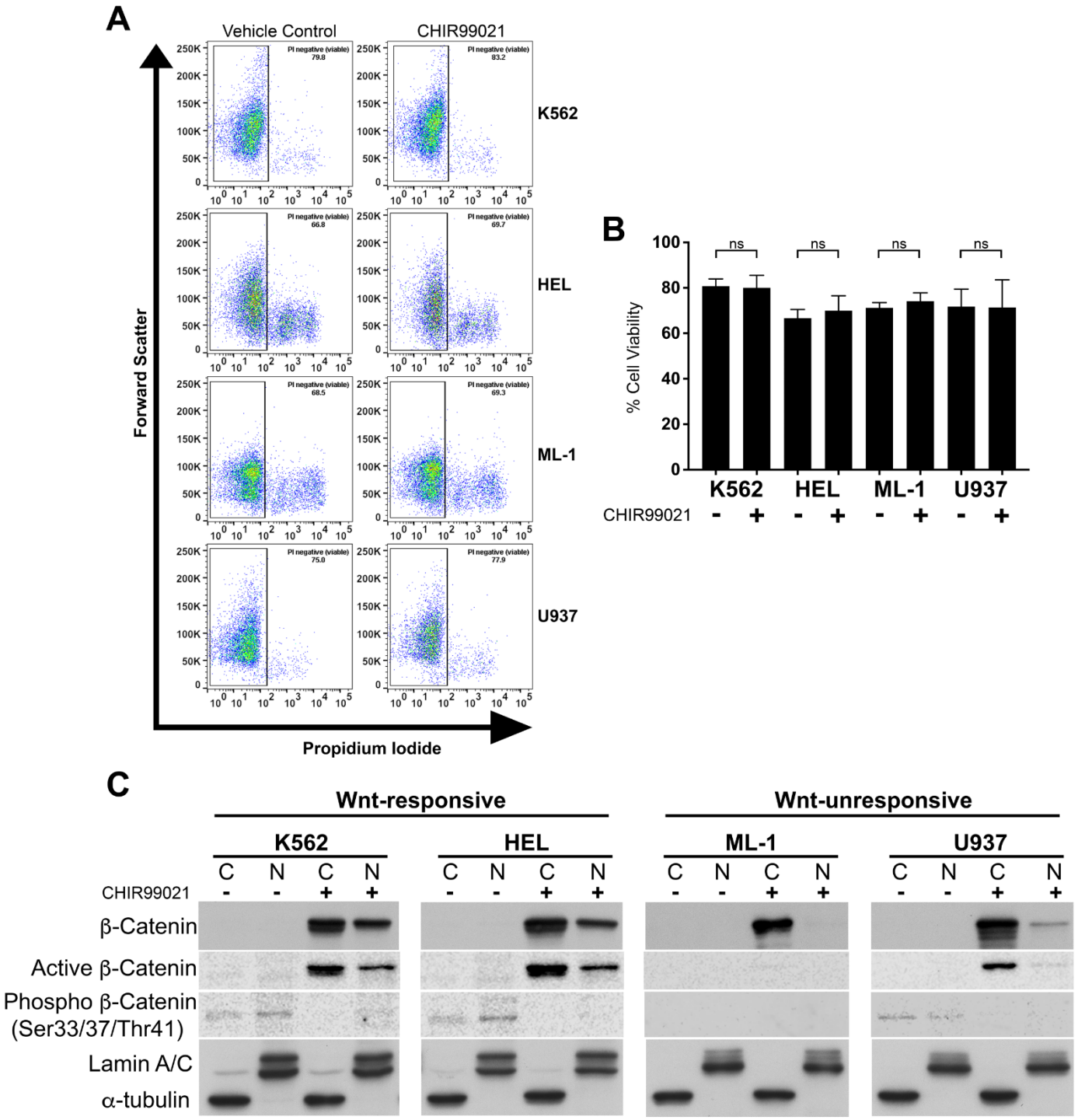

Supplementary Figure S1. Myeloid cell line viability and β-catenin phosphorylation variant expression in response to GSK3 inhibition. (**A**) Representative flow cytometric pseudocolor plots showing propidium staining for K562, HEL, ML-1 and U937 cells following 16hr 5μM CHIR99021 treatment. Percentage of events falling into PI negative gate (viable) are given in upper right of each plot. (**B**) Summary showing the percentage cell viability for each myeloid cell line following 16hr 5μM CHIR99021 treatment. (**C**) Representative immunoblots showing total β-catenin, active (non-phosphorylated) β-catenin and phosphorylated β-catenin (Ser33/37/Thr41) subcellular-localization in myeloid cells following CHIR99021 treatment (GSK3β inhibitor). Lamin A/C and α-tubulin indicate the purity/loading of the nuclear (N) and cytosol (C) fractions respectively. Data represents mean±1 SD, *n*=3, ns=not significant.

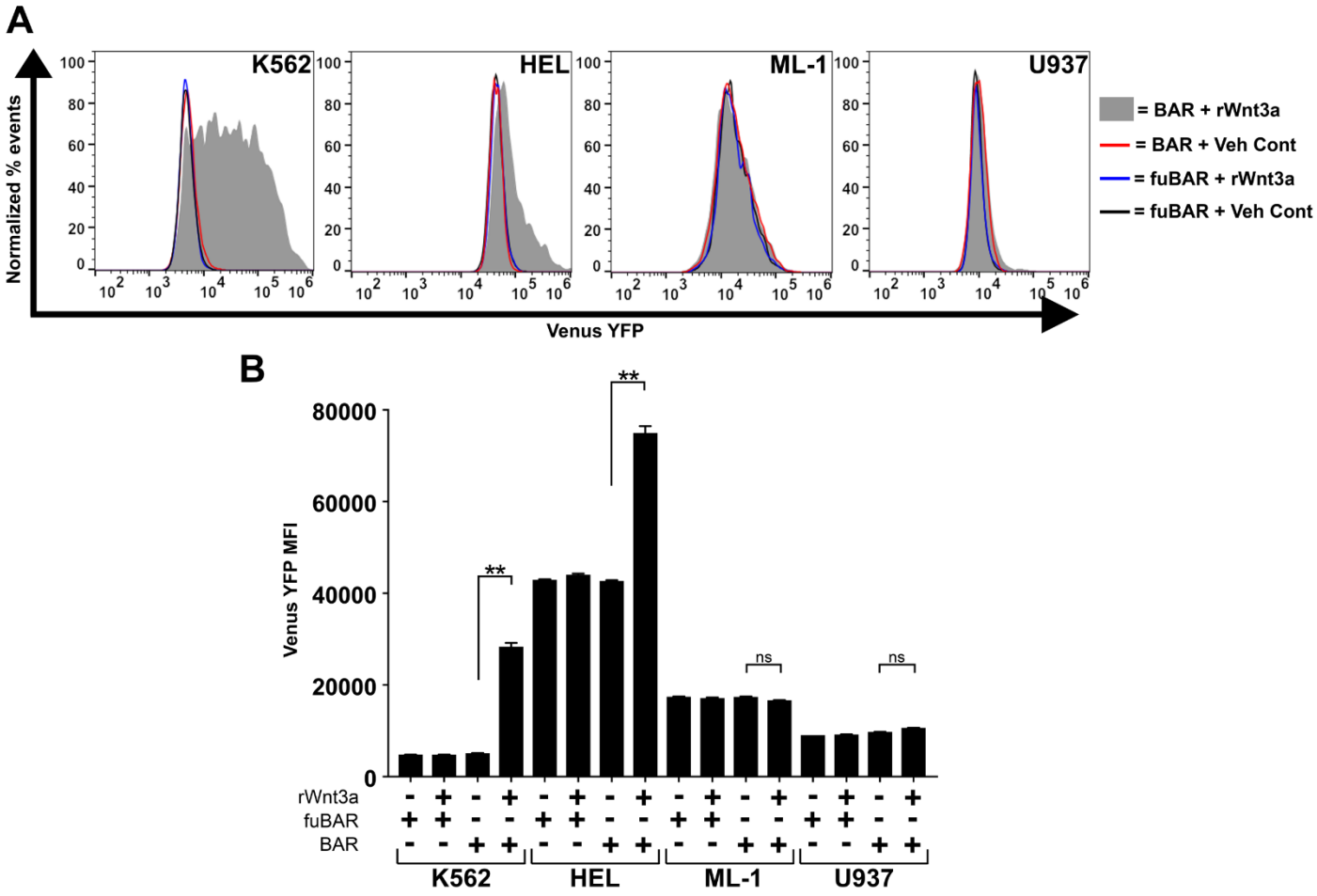

Supplementary Figure S2. Myeloid leukemia cell lines exhibit a heterogeneous response to Wnt stimulation with Wnt3a. (**A**) Representative flow cytometric histograms showing intensity of the TCF-dependent expression of YFP from the 'β-catenin activated reporter' (BAR) reporter, or negative control 'found unresponsive β-catenin activated reporter' (fuBAR) control (containing mutated promoter binding sites) following treatment with rWnt3a/vehicle control (PBS/0.1% BSA) for 16hr. (**B**) Summary showing the median fluorescence intensity generated from the BAR/fuBAR reporters in myeloid cell lines treated ± rWnt3a. Data represents mean±1 SD, statistical significance is denoted by ***P*<0.01 and ns=not significant.

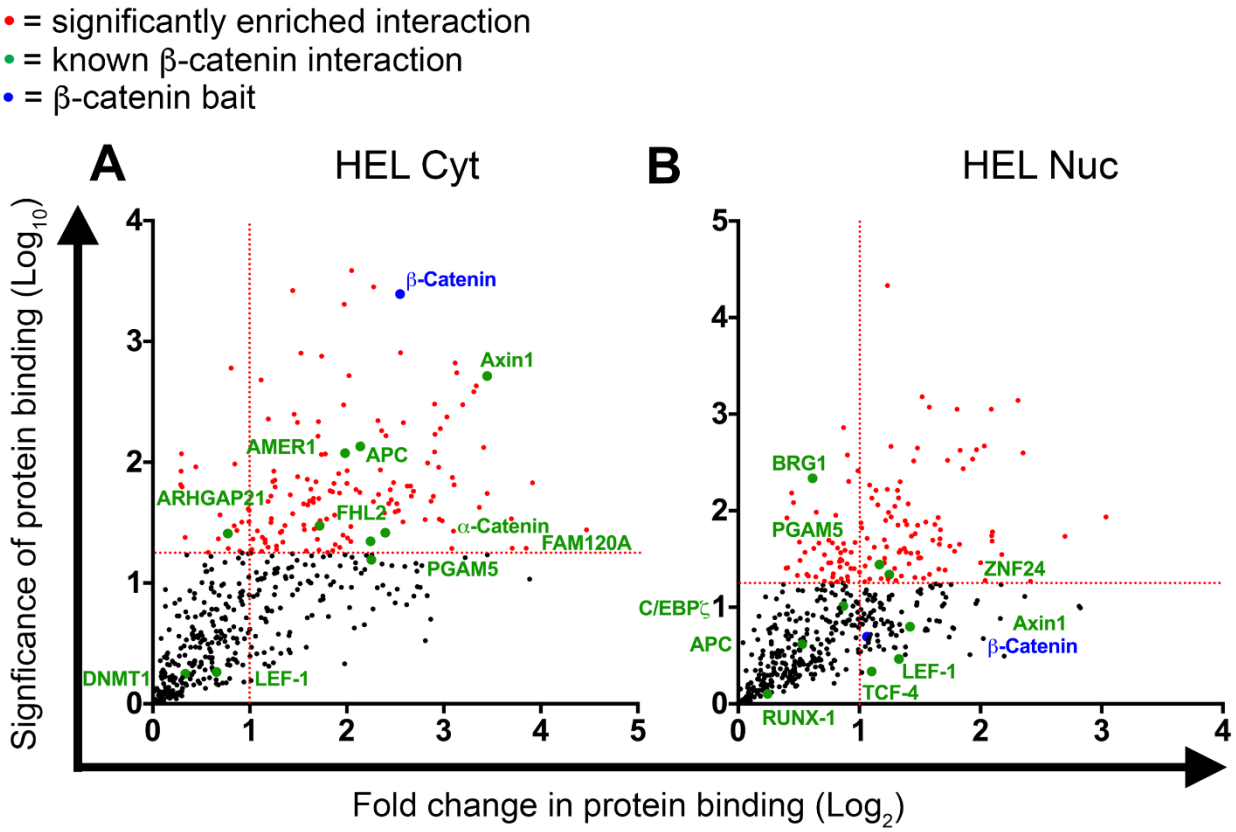

Supplementary Figure S3. Proteomics analyses reveal rich β-catenin interaction networks in Wnt-responsive HEL cells. Scatter plots showing summary of β-catenin protein interactions detected in HEL (**A**) cytosolic, and (**B**) nuclear fractions (n=3). Vertical dashed red line indicates the threshold for 2-fold change in protein binding at $\log_2$ (=1) relative to IgG Co-IP. Horizontal red line represents threshold for significant interactions at p=0.05 on $\log_{10}$ scale (=1.3). Highlighted red dots indicate all statistically significant interactions, blue dot indicates position of β-catenin bait and green highlighted events/labels indicate known enriched interactions/associations for β-catenin. Remaining black dots represent other proteins detected in the MS analysis. Fold change values less than 0 are not shown because these likely represent contaminants (see Supplementary material).

Supplementary Table S2. List of novel β-catenin interactions observed in K562 and ML1 cytosolic and nuclear fractions. Significant proteins only are shown, and specificity was defined as proteins detected in 10% or less of the 411-affinity purified mass spectrometry datasets present in the CRAPome database. Known interactions were removed from the analysis. Proteins are ranked according to statistical significance of protein binding. Threshold for 2-fold change in protein binding (relative to IgG Co-IP) at $\log_2 = 1$, whilst threshold for significant interactions at p=0.05 on $\log_{10}$ scale = 1.3.

Significance of protein binding (-Log10 *t*-test p value)	Fold change in protein binding (Log2)	Gene name	CRAPome frequency (/411)
K562 Cytosol			
3.77	3.01	CPEB4	1
2.95	1.52	DDX20	40
2.78	1.95	MRPS17	11
2.58	3.03	PRKRA	23
2.42	1.78	IGHMBP2	8
2.35	0.41	APOBEC3B	9
2.25	2.13	MRPS23	21
2.22	1.99	TRIM25	29
2.09	0.72	ABCF2	24
2.08	2.30	DHX36	23
2.07	0.56	MRPL1	13
2.06	1.85	FASTK	0
2.01	2.78	ZC3H7A	5
2.01	1.89	PPHLN1	32
1.95	1.62	EIF2AK2	14
1.93	0.98	FLJ13612	24
1.91	1.02	MRPS15	15
1.89	2.07	UPF1	35
1.87	1.08	MRPL11	11
1.87	0.33	DDX24	40
1.86	1.42	ZC3H7B	2
1.82	2.06	MRPL2	22
1.81	1.37	ZNF346	2
1.78	1.48	MRPL27	14
1.74	0.69	MBD3	32
1.74	0.46	NOL11	25
1.70	1.01	TOE1	21
1.69	1.88	MSI2	13
1.68	0.96	XRN1	26
1.62	2.39	AP2M1	21
1.61	3.12	ZCCHC3	8
1.61	1.18	MRPS22	32
1.58	2.57	DROSHA	10
1.57	0.36	FYTTD1	13
1.53	2.73	MRPL15	13
1.53	0.46	NXF2B	0
1.51	1.19	FAM83A	0
1.51	2.09	PURA	27
1.46	0.74	HNRNPLL	21
1.43	0.66	PNAS-3	34
1.43	2.00	PCM1	31
1.43	1.17	APOBEC3F	17
1.41	1.64	CELF1	10
1.40	1.26	LARP1B	36
1.37	1.72	BMP2K	0
1.36	1.98	MRPS34	24
1.35	1.42	RBM45	2
1.34	0.61	ASCC3	39
1.33	2.60	STAU2	32
1.32	2.27	AP2A1	24
1.31	2.14	AP2M1	21
1.31	1.37	RBM7	23
1.30	0.68	WDR76	8
1.28	3.01	APOBEC3G	0
1.27	1.51	MRPS2	19
1.26	1.66	ARHGAP21	21
1.26	1.76	DAP3	41
K562 Nucleus			
2.17	0.47	LIN28B	10
2.06	0.42	DDX24	40
2.01	0.58	ZCCHC9	2
1.96	0.71	UTP20	12

1.86	0.28	PRC1	22
1.81	0.48	MRPS24	2
1.65	0.50	POP1	40
1.61	0.56	INTS6	1
1.60	0.27	ABCF2	24
1.56	0.61	DECR1	15
1.54	1.58	RBM45	2
1.52	1.35	NCOA5	19
1.50	0.59	UTP3	23
1.45	0.54	DAP3	41
1.41	0.51	NOL9	34
1.38	0.34	RRP1B	21
1.35	0.61	MYBBP1A	3
1.32	0.48	HNRPUL1	0
1.30	0.89	HNRNPH1	30
1.30	0.41	DDX10	14
1.27	0.39	GNL2	32
1.26	0.42	MBD3	13
1.26	0.29	EXOSC9	2
1.25	0.29	TIMM21	0
ML1 Cytosol			
2.62	2.56	KRT34	28
2.60	0.82	PPIF	28
2.58	1.14	CLTB	14
2.12	0.30	ADRBK1	0
1.79	0.43	ATP6V1E1	16
1.75	0.52	NXF1	38
1.55	0.43	RBM15	40
1.52	0.60	PIK3R1	5
1.44	0.28	RAB5B	40
1.41	0.39	HMGN5	9
1.32	1.07	CENPV	26
1.26	1.22	FABP5	38
ML1 Nucleus			
2.41	0.06	INPP5D	0
1.79	0.92	PNP	36
1.44	0.40	TMX1	23
1.43	0.18	RBM15	40
1.42	0.31	HBS1L	32
1.41	0.75	CDV3	26
1.34	0.30	BUD31	28

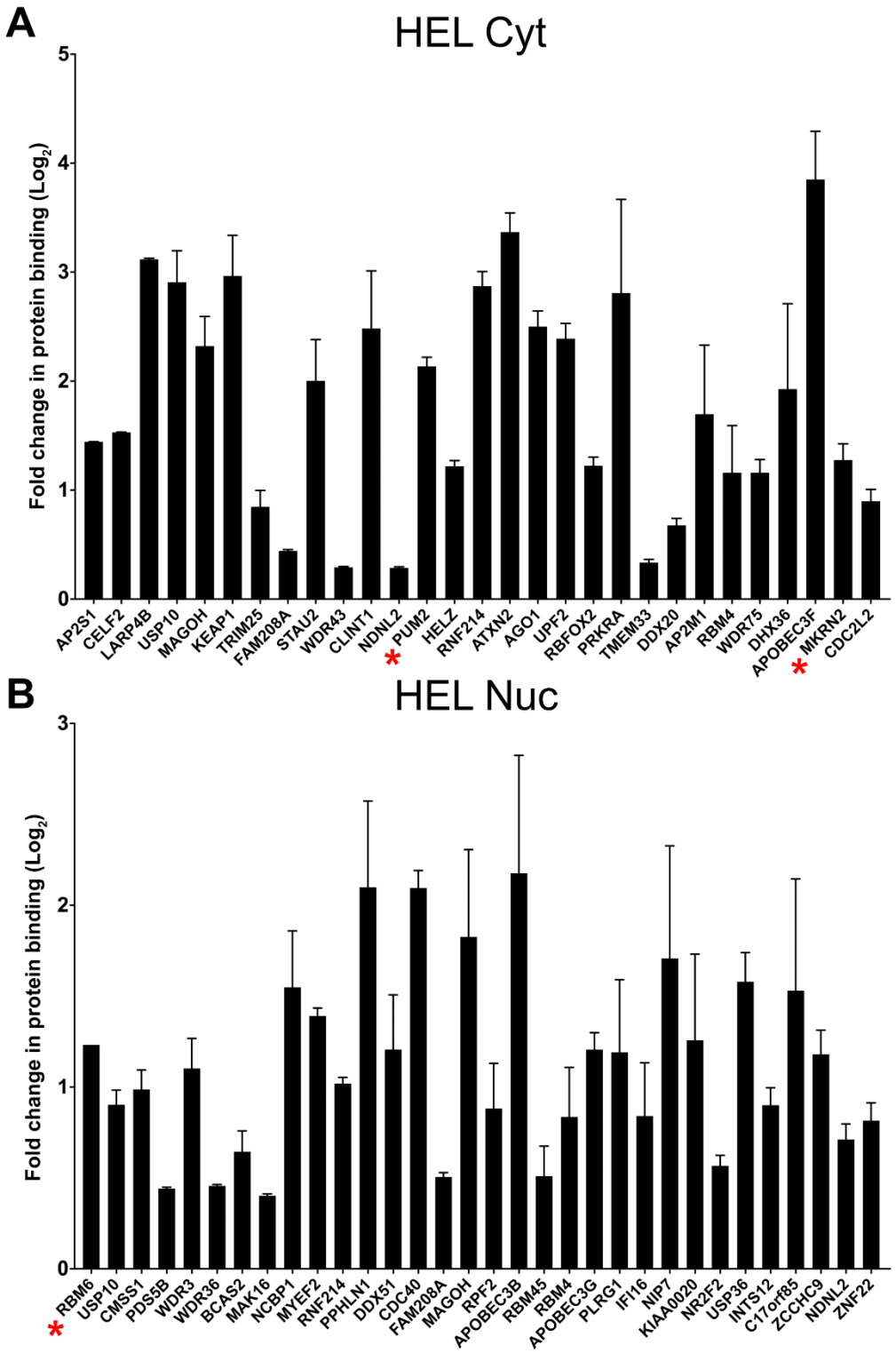

Supplementary Figure S4. Mass spectrometric analyses identify putative novel interaction partners for β-catenin in HEL cells. Bar graphs summarising the average fold change in protein binding (relative to matched IgG co-IP) for novel β-catenin interactions observed in HEL (**A**) cytosolic and (**B**) nuclear fractions. Significant proteins only are shown (red dots in Supplementary Figure S1 panels) with a frequency on the CRAPome database of ≤10% and known interactions were removed. Red asterisks represent proteins of particular significance to myeloid leukemias and/or Wnt signaling (discussed further in results section). Proteins are ranked along X-axis according to statistical significance (left = most significant); see also Supplementary Table S3.

Supplementary Table S3. List of novel β-catenin interactions observed in HEL cytosolic and nuclear fractions. Significant proteins only are shown, and specificity was defined as proteins detected in 10% or less of the 411-affinity purified mass spectrometry datasets present in the CRAPome database. Known interactions were removed from the analysis. Proteins are ranked according to statistical significance of protein binding. Threshold for 2-fold change in protein binding (relative to IgG Co-IP) at $\log_2$ =1, whilst threshold for significant interactions at p=0.05 on $\log_{10}$ scale =1.3.

Significance of protein binding (-Log10 *t*-test p value)	Fold change in protein binding (Log2)	Gene name	CRAPome frequency (/411)
HEL Cytosol			
3.42	1.44	AP2S1	1
2.90	1.53	CELF2	4
2.82	3.12	LARP4B	20
2.48	2.91	USP10	35
2.35	2.32	MAGOH	37
2.28	2.96	KEAP1	30
1.99	0.85	TRIM25	29
1.96	0.44	FAM208A	37
1.93	2.00	STAU2	32
1.93	0.29	WDR43	27
1.83	2.48	CLINT1	40
1.81	0.29	NDNL2	0
1.75	2.14	PUM2	22
1.72	1.22	HELZ	9
1.68	2.87	RNF214	2
1.63	3.37	ATXN2	33
1.59	2.50	AGO1	14
1.58	2.39	UPF2	0
1.53	1.22	RBFOX2	14
1.52	2.81	PRKRA	23
1.38	0.33	TMEM33	34
1.37	0.68	DDX20	40
1.36	1.70	AP2M1	21
1.36	1.16	RBM4	33
1.33	1.16	WDR75	15
1.29	1.93	DHX36	23
1.29	3.85	APOBEC3F	17
1.28	1.28	MKRN2	3
1.26	0.90	CDC2L2	39
HEL Nuclear			
4.33	1.23	RBM6	25
2.58	0.90	USP10	35
2.41	0.99	CMSS1	6
2.18	0.44	PDS5B	8
2.13	1.10	WDR3	20
2.08	0.46	WDR36	41
1.98	0.64	BCAS2	40
1.93	0.40	MAK16	13
1.88	1.55	NCBP1	38
1.86	1.39	MYEF2	16
1.82	1.02	RNF214	2
1.78	2.10	PPHLN1	32
1.70	1.21	DDX51	10
1.69	2.09	CDC40	15
1.67	0.51	FAM208A	37
1.65	1.83	MAGOH	37
1.59	0.88	RPF2	27
1.55	2.18	APOBEC3B	9
1.48	0.51	RBM45	2
1.47	0.84	RBM4	33
1.46	1.21	APOBEC3G	0
1.45	1.19	PLRG1	38
1.42	0.84	IFI16	9
1.38	1.71	NIP7	16
1.36	1.26	KIAA0020	16
1.34	0.57	NR2F2	4

1.34	1.58	USP36	26
1.32	0.90	INTS12	14
1.30	1.53	C17orf85	22
1.30	1.18	ZCCHC9	2
1.27	0.71	NDNL2	0
1.27	0.81	ZNF22	2

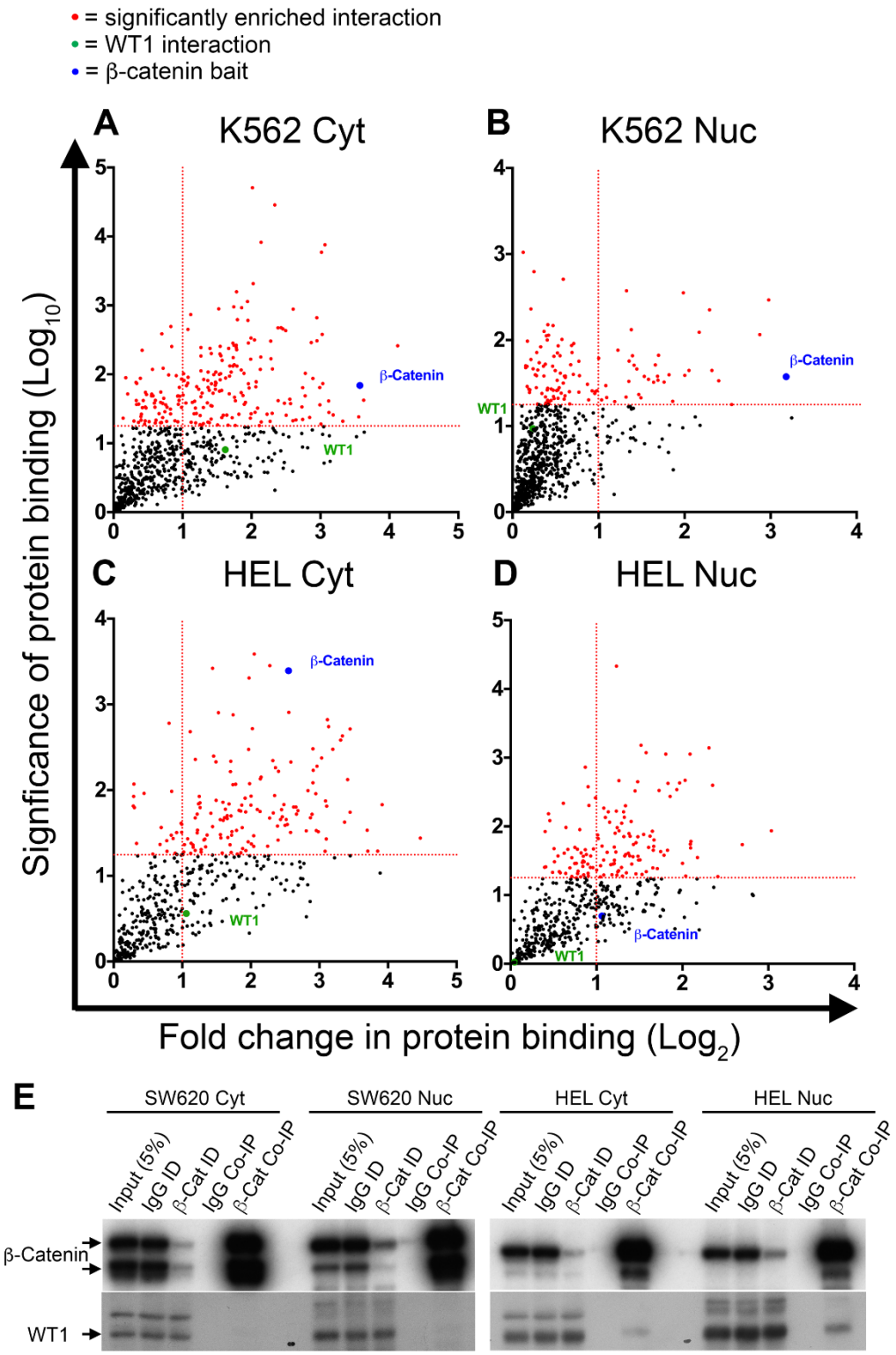

Supplementary Figure S5. Proteomics analyses reveal β-catenin interaction with WT1 in myeloid leukemia cells. Scatter plots showing summary of β-catenin protein interactions detected in (**A**) K562 cytosolic, (**B**) K562 nuclear, (**C**) ML1 cytosolic, and (**D**) ML1 nuclear fractions. Vertical dashed red line indicates the threshold for 2-fold change in protein binding at $\log_2$ (=1) relative to IgG co-IP. Horizontal red line represents threshold for significant interactions at p=0.05 on $\log_{10}$ scale (=1.3). Highlighted red dots indicate all statistically significant interactions, blue dot indicates position of β-catenin bait and green dot indicates position of WT1. Remaining black dots represent other proteins detected in the MS analysis. (**E**) Representative immunoblots showing β-catenin and WT1 protein level from β-catenin co-IPs pulled down from the cytosol or nucleus of SW620 or HEL cells (ID=immunodepleted). Note the absence of WT1 detection in SW620 fractions highlighting potential context dependence of interaction.

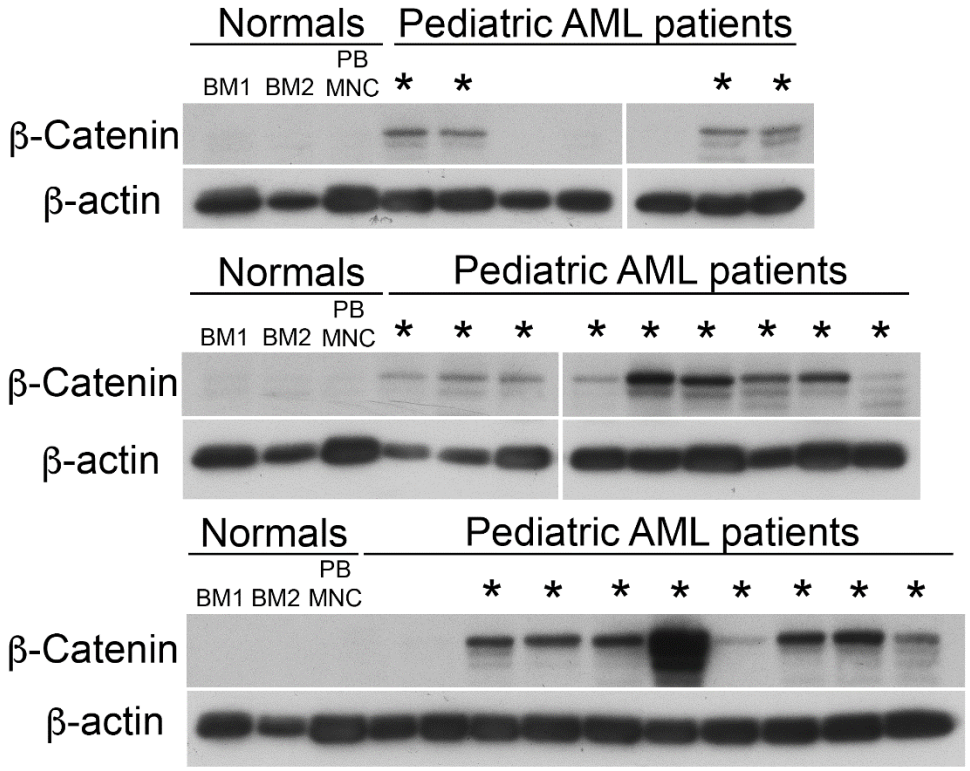

Supplementary Figure S6. Expression of β-catenin protein in pediatric AML samples. Immunoblot screen of 26 primary pediatric AML patient samples showing level of total cell β-catenin compared with normal bone marrow (BM) or peripheral blood mononuclear cells (PB MNC). * samples overexpressing β-catenin protein (~80%) versus levels observed in normal BM or PB MNC. Interestingly, we observed a much higher overall incidence of β-catenin protein overexpression amongst our pediatric AML cohort (Supplemental Figure S4) versus previous estimates for adult AML (~20-60%; see supplemental references).[1-3] This is in keeping with a recent study which examined the molecular landscape of pediatric AML, and found a higher proportion of aberrations which impact Wnt signaling relative to adult AML.[4] *Mixed-lineage leukemia* (*MLL*) gene rearrangements are also more prevalent in childhood AML and this model of leukemogenesis has been shown to require β-catenin for malignant transformation.[5-7] Detection of β-actin was used to assess protein loading.

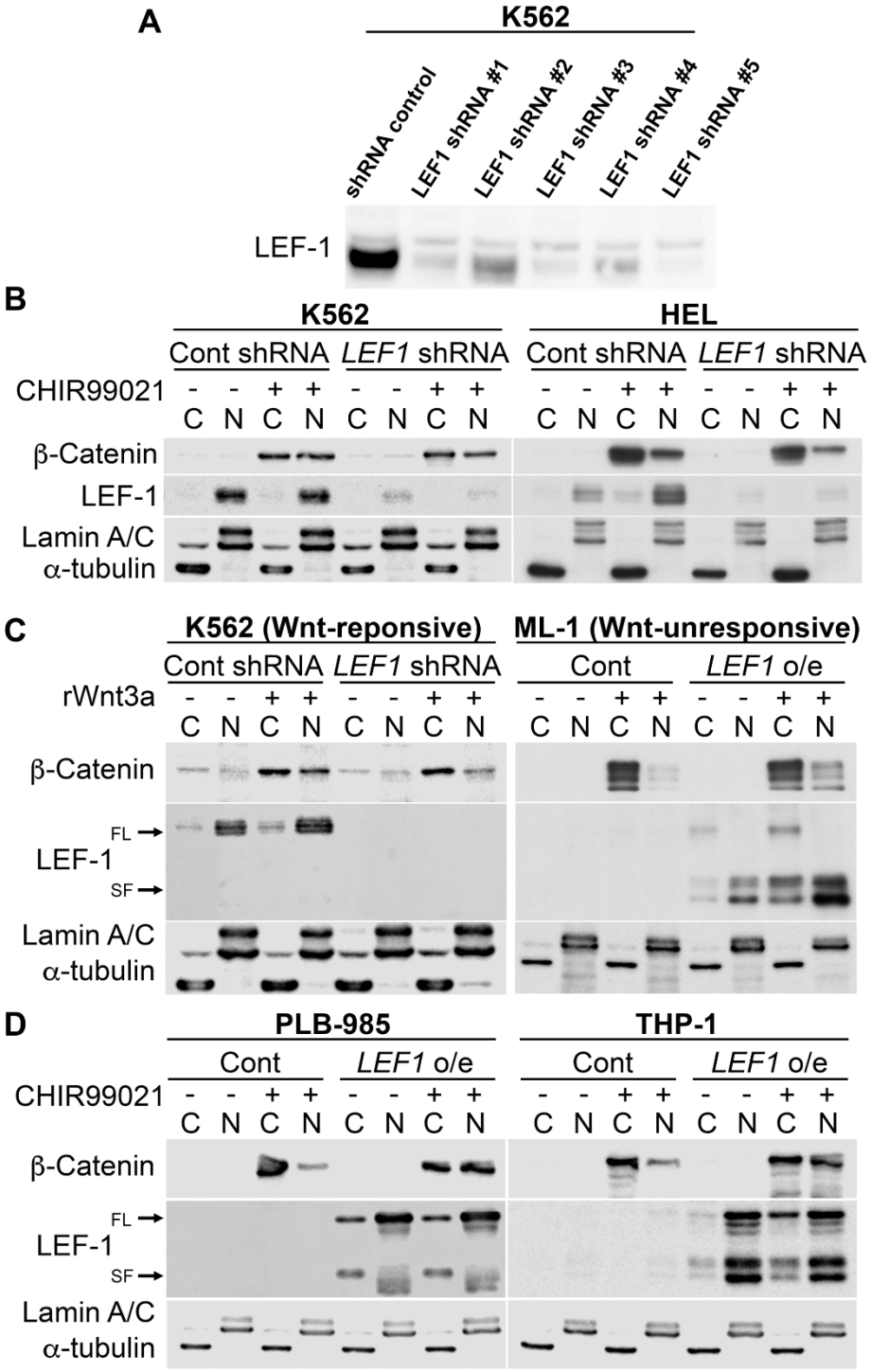

Supplementary Figure S7. Modulation of LEF-1 expression affects relative nuclear β-catenin level. (**A**) Immunoblots showing LEF-1 protein expression level in K562 cells following lentiviral transduction with a panel of 5 human LEF-1 targeted shRNAs (#1 = TRCN0000-020163, #2 = -413476, #3 = -418104, #4= -428178 and #5= -428355). Since LEF-1 shRNA #5 exhibited optimal LEF-1 protein reduction, this was used preferentially through the study. (**B**) Immunoblots showing the level and subcellular localization of β-catenin in K562/HEL cells in response to an alternative LEF-1 shRNA (#3). (**C**) Immunoblots showing the level and subcellular localization of β-catenin in representative Wnt-responsive cells (K562; exhibiting LEF-1 knockdown) and Wnt-unresponsive cells (ML-1; exhibiting LEF-1 overexpression) following Wnt3a exposure. The positions of full-length (FL) and short-forms (SF) of LEF-1 protein on the blot are indicated by arrows. (**D**) Immunoblots showing the level and subcellular localization of β-catenin in PLB-985 and THP-1 cells in response to control/*LEF1* overexpression (o/e) ± 16 hr CHIR99021 treatment. Lamin A/C and α-tubulin were used to assess fraction purity and protein loading.

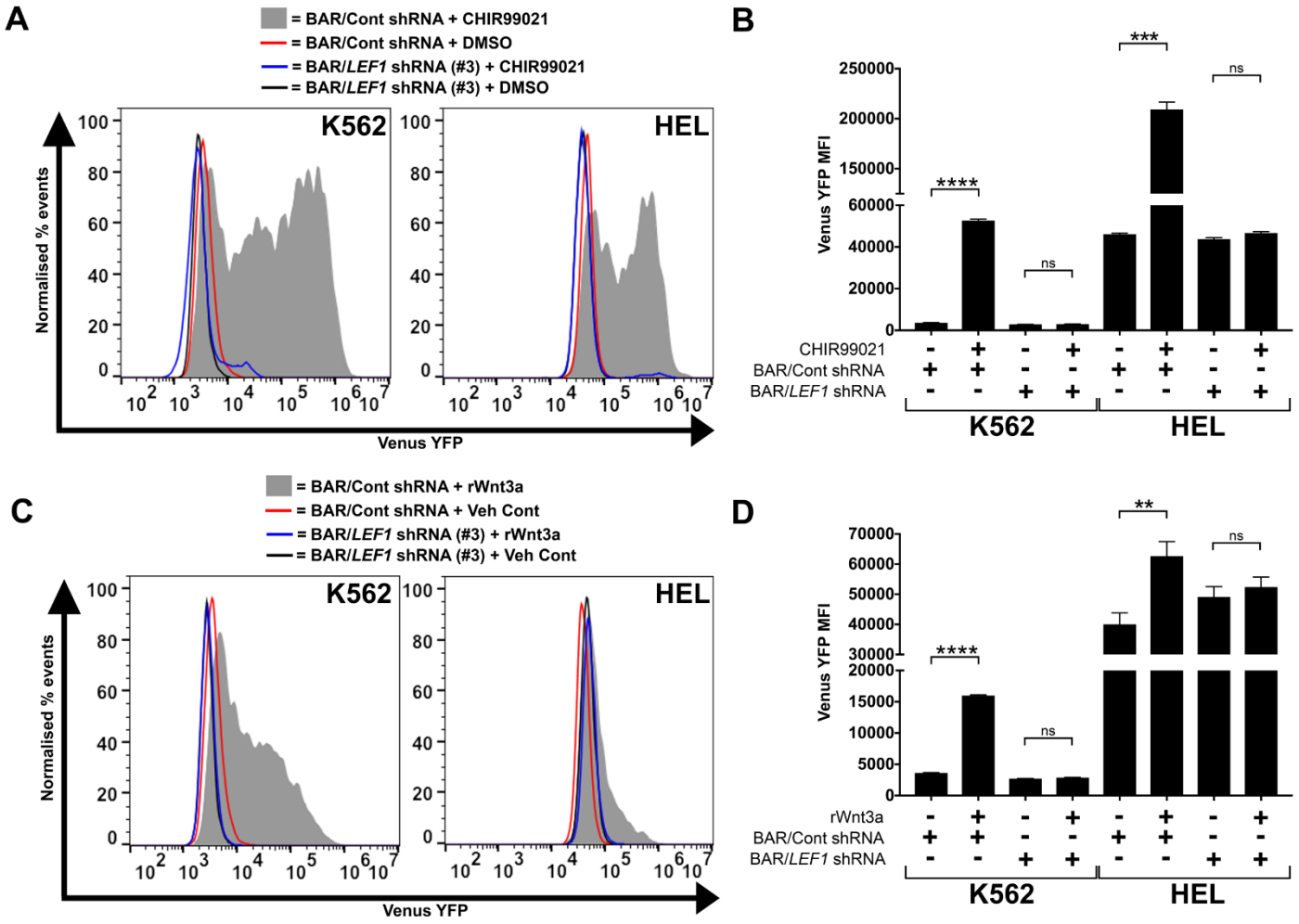

Supplementary Figure S8. Modulation of LEF-1 expression affects downstream Wnt signalling. (**A**) Representative flow cytometric histograms showing intensity of the TCF reporter (BAR) in K562 and HEL cells treated with an alternative *LEF1* shRNA (#3) ± CHIR99021. (**B**) Summary data showing the median fluorescence intensity generated from the BAR reporter in K562 and HEL cells treated with an alternative *LEF1* shRNA (#3) ± CHIR99021. (**C**) Representative flow cytometric histograms showing intensity of the BAR reporter in K562 and HEL cells treated with an alternative *LEF1* shRNA (#3) ± rWnt3a. (**D**) Summary data showing the median fluorescence intensity generated from the BAR reporter in K562 and HEL cells treated with an alternative *LEF1* shRNA (#3) ± rWnt3a. Data represents mean±1 SD, statistical significance is denoted by ***P*<0.01, ****P*<0.001, *****P*<0.0001 and ns=not significant.

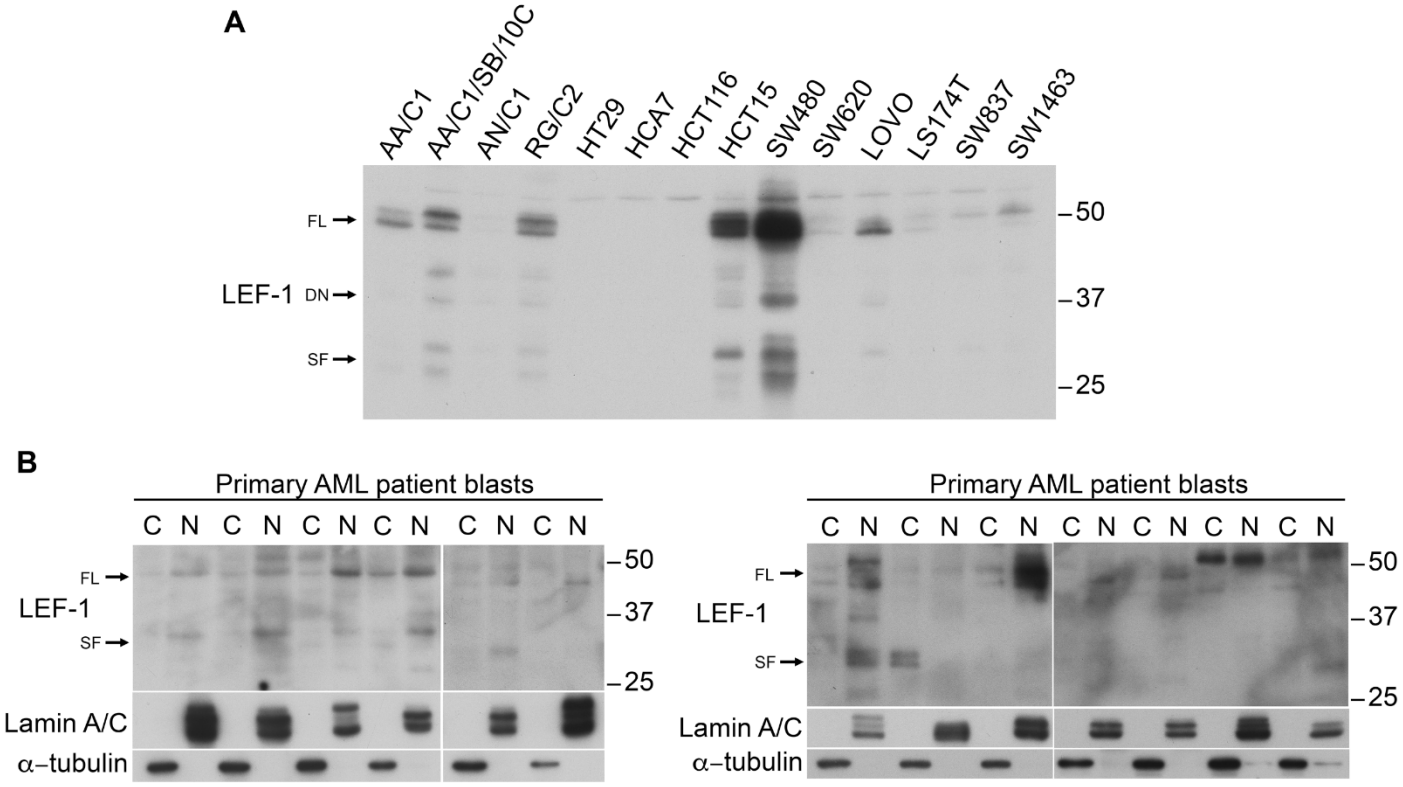

Supplementary Figure S9. Short forms of LEF-1 protein are observed in CRC cell lines and primary AML samples. (**A**) Immunoblot screen of 14 colorectal adenoma or cancer cell lines showing abundance of different LEF-1 protein forms. The positions of full-length (FL), dominant-negative isoforms (DN) and short-forms (SF) of LEF-1 protein are indicated by arrows. The loading control for this blot has previously been published elsewhere.[8] (**B**) Extended immunoblots showing the cytosolic and nuclear expression of LEF-1 protein forms in the primary AML patient samples featured in Figure 5. Lamin A/C and α-tubulin were used to assess fractionation efficiency and equal protein loading.

1. Chen CC, Gau JP, You JY, Lee KD, Yu YB, Lu CH*, et al.* Prognostic significance of beta-catenin and topoisomerase IIalpha in de novo acute myeloid leukemia. *AmJHematol* 2009; **84**(2)**:** 87-92.
2. Ysebaert L, Chicanne G, Demur C, De TF, Prade-Houdellier N, Ruidavets JB*, et al.* Expression of beta-catenin by acute myeloid leukemia cells predicts enhanced clonogenic capacities and poor prognosis. *Leukemia* 2006; **20**(7)**:** 1211-1216.
3. Xu J, Suzuki M, Niwa Y, Hiraga J, Nagasaka T, Ito M*, et al.* Clinical significance of nuclear non-phosphorylated beta-catenin in acute myeloid leukaemia and myelodysplastic syndrome. *BrJHaematol* 2008; **140**(4)**:** 394-401.
4. Bolouri H, Farrar JE, Triche T, Jr., Ries RE, Lim EL, Alonzo TA*, et al.* The molecular landscape of pediatric acute myeloid leukemia reveals recurrent structural alterations and age-specific mutational interactions. *Nat Med* 2017.
5. Wang Y, Krivtsov AV, Sinha AU, North TE, Goessling W, Feng Z*, et al.* The Wnt/beta-catenin pathway is required for the development of leukemia stem cells in AML. *Science* 2010; **327**(5973)**:** 1650-1653.
6. Yeung J, Esposito MT, Gandillet A, Zeisig BB, Griessinger E, Bonnet D*, et al.* beta-Catenin mediates the establishment and drug resistance of MLL leukemic stem cells. *Cancer Cell* 2010; **18**(6)**:** 606-618.
7. Dietrich PA, Yang C, Leung HH, Lynch JR, Gonzales E, Liu B*, et al.* GPR84 sustains aberrant beta-catenin signaling in leukemic stem cells for maintenance of MLL leukemogenesis. *Blood* 2014; **124**(22)**:** 3284-3294.
8. Legge DN, Shephard AP, Collard TJ, Greenhough A, Chambers AC, Clarkson RW, *et al*. BCL-3 enhances β-catenin signalling in colorectal tumour cells promoting a cancer stem cell phenotype. *bioRxiv* doi: 10.1101/178004.

Supplementary Methods

Cross-linking of antibodies for co-immunoprecipitation

For co-immunoprecipitation, 8μg of β-catenin (Clone 14)/IgG (Clone MOPC-31C) antibody (Becton Dickinson, Oxford, UK) was crosslinked to Protein G Dynabeads® (Thermo Fisher Scientific, Loughborough, UK) for 2h at room temperature. Following washing, bound β-catenin/IgG antibody was crosslinked to Protein G Dynabeads® in coupling buffer (0.2M triethanolamine (Sigma-Aldrich) in PBS with 0.01% Tween-20 (pH9), 20mM Dimethyl pimelimidate dihydrochloride (Sigma-Aldrich) for 1 h at room temperature. Following washing, crosslinked β-catenin/IgG antibody was quenched (50mM ethanolamine (Sigma-Aldrich) in PBS with 0.01% Tween-20) for 30min at room temperature, followed by washing in elution buffer (0.2M glycine (Sigma-Aldrich) pH2.5 with 0.01% Tween-20) to remove uncrosslinked antibody.

TMT Labelling and High pH reversed-phase chromatography

Immunoprecipitated samples (eight samples per experiment) were digested on the beads with trypsin (2.5μg trypsin; 37°C, overnight), labelled with Tandem Mass Tag (TMT) ten-plex reagents according to the manufacturer's protocol (Thermo Fisher Scientific) and the labelled samples pooled. The pooled sample was evaporated to dryness, resuspended in 5% formic acid and then desalted using a SepPak cartridge according to the manufacturer's instructions (Waters, Milford, Massachusetts, USA). Eluate from the SepPak cartridge was again evaporated to dryness and resuspended in buffer A (20 mM ammonium hydroxide, pH 10) prior to fractionation by high pH reversed-phase chromatography using an Ultimate 3000 liquid chromatography system (Thermo Fisher Scientific). In brief, the sample was loaded onto an XBridge BEH C18 Column (130Å, 3.5 μm, 2.1 mm X 150 mm, Waters, UK) in buffer A and peptides eluted with an increasing gradient of buffer B (20 mM Ammonium Hydroxide in acetonitrile, pH 10) from 0-95% over 60 min. The resulting fractions were evaporated to dryness and resuspended in 1% formic acid prior to analysis by nano-LC MSMS.

Nano-LC Mass Spectrometry

High pH RP fractions were further fractionated using an Ultimate 3000 nano-LC system in line with an Orbitrap Fusion Tribrid mass spectrometer (Thermo Scientific). In brief, peptides in 1% (*v/v*) formic acid were injected onto an Acclaim PepMap C18 nano-trap column (Thermo Scientific). After washing with 0.5% (*v/v*) acetonitrile 0.1% (*v/v*) formic acid peptides were resolved on a 250 mm × 75 μm Acclaim PepMap C18 reverse phase analytical column (Thermo Scientific) over a 150 min organic gradient, using 7 gradient segments (1-6% solvent B over 1 min, 6-15% B over 58 min, 15-

32% B over 58 min, 32-40% B over 5 min, 40-90% B over 1 min, held at 90% B for 6 min and then reduced to 1% B over 1 min) with a flow rate of 300 nl/min. Solvent A was 0.1% formic acid and Solvent B was aqueous 80% acetonitrile in 0.1% formic acid. Peptides were ionized by nano-electrospray ionization at 2.0kV using a stainless-steel emitter with an internal diameter of 30 μm (Thermo Scientific) and a capillary temperature of 275°C. All spectra were acquired using an Orbitrap Fusion Tribrid mass spectrometer controlled by Xcalibur 2.0 software (Thermo Scientific) and operated in data-dependent acquisition mode using an SPS-MS3 workflow. FTMS1 spectra were collected at a resolution of 120 000, with an automatic gain control (AGC) target of 200 000 and a max injection time of 50ms. Precursors were filtered with an intensity threshold of 5000, according to charge state (to include charge states 2-7) and with monoisotopic precursor selection. Previously interrogated precursors were excluded using a dynamic window (60s +/-10ppm). The MS2 precursors were isolated with a quadrupole mass filter set to a width of 1.2m/z. ITMS2 spectra were collected with an AGC target of 10 000, max injection time of 70ms and CID collision energy of 35%. For FTMS3 analysis, the Orbitrap was operated at 50 000 resolution with an AGC target of 50 000 and a max injection time of 105ms. Precursors were fragmented by high energy collision dissociation (HCD) at a normalized collision energy of 60% to ensure maximal TMT reporter ion yield. Synchronous Precursor Selection (SPS) was enabled to include up to 5 MS2 fragment ions in the FTMS3 scan.

Mass spectrometry Data Analysis

The raw data files were processed and quantified using Proteome Discoverer software v1.4 (Thermo Scientific) and searched against the UniProt Human database (134169 entries downloaded 18/4/2016) using the SEQUEST algorithm. Peptide precursor mass tolerance was set at 10ppm, and MS/MS tolerance was set at 0.6Da. Search criteria included oxidation of methionine (+15.9949) as a variable modification and carbamidomethylation of cysteine (+57.0214) and the addition of the TMT mass tag (+229.163) to peptide N-termini and lysine as fixed modifications. Searches were performed with full tryptic digestion and a maximum of 1 missed cleavage was allowed. The reverse database search option was enabled and all peptide data was filtered to satisfy false discovery rate (FDR) of 1%.

β-Catenin and LEF-1 densitometry

Densitometry was performed using ImageJ software v2.0.0-rc-43/1.51s (National Institutes of Health, Bethesda, MD, USA) and arbitrary densitometric units used to calculate relative nuclear β-catenin/LEF-1 localization. Relative percentage nuclear localization was calculated by normalizing the β-catenin or LEF-1 protein level to the α-tubulin or lamin A/C protein level present in the

respective cytosolic or nuclear fraction, followed by calculation of the nuclear β-catenin or LEF-1 present as a proportion of the total β-catenin or LEF-1 level.

Supplementary MS data (see associated Excel file).

Raw and processed tandem mass tag (TMT) mass spectrometry data obtained from β-catenin co-IP's from K562, HEL, ML-1 and SW620 cytoplasm and nuclear fractions. These data can also be found deposited to the ProteomeXchange Consortium (http://proteomecentral.proteomexchange.org) via the PRIDE partner repository with the dataset identifier PXD009305. Parameter definitions and data sheet types are explained within the first sheets of the excel file.